Future Technology
Open Access Journal
ISSN 2832-0379

November 2026| Volume 05 | Issue 04 | Pages 146-156

Journal homepage: https://fupubco.com/futech

https://doi.org/10.55670/fpll.futech.5.4.12

Future Publishing LLC

Article

Wireless sensor network-based real-time monitoring system for large ship airbag launching: design and field validation

Ji Chen[1,2], Saiful Bahri Bin Mohamed[1]*, W Noor Fatihah W.Mohamad[1], Al Khowarizmi[3], Rongtao Yang[4]

[1]Faculty of Innovative Design and Technology, Universiti Sultan Zainal Abidin, Terengganu 23000, Malaysia
[2]School of Mechanical Engineering and Automation, Bohai Shipbuilding Vocational College, Huludao 125105, China
[3]Faculty of Computer Science and Information Technology, Universitas Muhammadiyah Sumatera Utara, Medan 20212, Indonesia
[4]Anhui Port & Shipping Sealand Equipment Co., Ltd., Tongling 246700, China

ARTICLE INFO

Article history:
Received 17 March 2026
Received in revised form
12 July 2026
Accepted 18 August 2026

Keywords:
Computational ship airbag launching, WSN, Inertial measurement units, Pressure sensors, Zigbee mesh communication architecture

*Corresponding author
Email address:
saifulbahri@unisza.edu.my

DOI: 10.55670/fpll.futech.5.4.12

ABSTRACT

Traditional monitoring solutions for airbag launching of large ships rely on mechanical pressure gauges with limited spatial coverage, slow response times (from several hundred milliseconds to a few seconds), and an inability to monitor dynamically changing attitude parameters during the launching procedure. This paper introduces a WSN-based real-time monitoring solution that combines IMUs and pressure sensors installed at strategic positions on the ship hull and airbags. The solution uses the hierarchical Zigbee mesh with edge computing nodes and the TDMA protocol to deliver real-time, high-speed communication with low end-to-end latency, even under challenging shipyard conditions. The Kalman filter fuses multi-sensor data to provide comprehensive monitoring of pitch, roll, heave displacement, velocity, and acceleration. In-field validation tests have been performed on cargo ships with 1500-2000 DWT capacities during the actual launching process at cooperating shipyards. The system achieves a sampling rate of 100 Hz for inertial data and 50 Hz for pressure data, end-to-end latency under 60 ms (95%), and measurement accuracy of ±0.3° for attitude angles and ±1.5% full scale for pressure measurement. Comparative analysis showed that the proposed system outperforms traditional mechanical gauges with a 75% reduction in spatial blind spots (60%→15% hull coverage), 20–100× faster temporal resolution (50–100 Hz vs. 1–5 Hz), and an 85% reduction in installation time (3.0 h vs. 19.5 h).

1. Introduction

Shipbuilding has undergone significant technological advances, particularly in ship launching systems. Airbag launching systems have gained attention from shipyards with limited facilities, as they use high-strength rubber bags placed under the ship to facilitate sliding into water along an inclined ramp [1-3]. Traditional monitoring approaches rely on pressure sensors at fixed locations within the airbag system [4]. However, these methods have major limitations. First, sparse sensor placement creates blind spots, preventing measurement of pressure variations across the ship-airbag interface [5]. Second, response times of hundreds of milliseconds to several seconds are too slow to capture transient events during launching [6]. Third, conventional sensors cannot measure ship attitude angles [7]. Recent advances in wireless sensor networks and MEMS technology enable more comprehensive monitoring [8]. WSN systems offer flexibility, scalability, and elimination of cabling in industrial environments. Combining multi-axis IMUs with pressure sensors allows simultaneous acquisition of force distribution and kinematic data for complete launch dynamics analysis. Edge computing in sensor nodes enables decentralized data processing and reduces communication bandwidth requirements [9,10]. Prior research has addressed individual monitoring aspects. Zhou et al. [11] developed a strain gauge system for airbag launches but lacked attitude measurement and required wired communication. Jouhari et al. [12] implemented wireless pressure monitoring but omitted dynamic data. Fiber optic sensors provide high spatial resolution but require complex installation. No prior work has integrated wireless monitoring of airbag pressure distribution, ship attitude, and dynamic behavior in a unified system. This work develops and validates a WSN-based monitoring system for real-time data acquisition during large ship airbag launches (Figure 1). The system addresses the drawbacks of the current approach by providing a synchronized pressure map, 3D attitude angle, velocity, and acceleration measurements. The wireless mesh network topology ensures reliable communication in highly electromagnetic shipyards while conserving energy. Kalman filtering algorithms reduce environmental uncertainties. The three key aspects of the paper include: (1) the use of a hierarchical wireless sensor network design for launching an airbag from large ships, (2) the use of an inertial measurement unit and pressure sensors with edge computing capability for the collection of the real-time motion parameters of the ship, and (3) a high-performance TDMA-based Zigbee communication system.

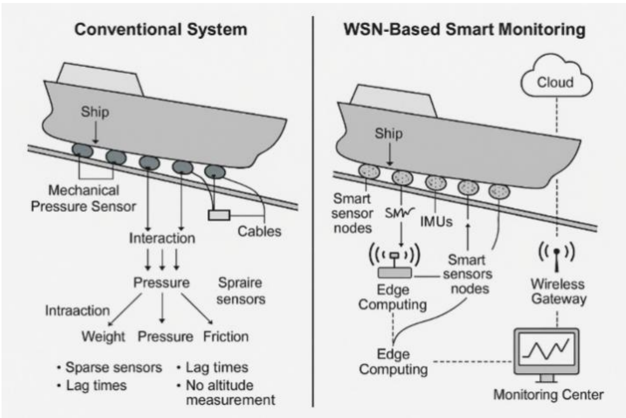

Figure 1. Conventional system VS WSN-based smart monitoring

2. System architecture design

2.1 Design objectives

The following key requirements play a significant role in designing the proposed system. It is essential to provide complete spatial coverage of both the ship hull and the airbags during the launch phase to avoid missing measurements at any stage of the experiment. The real-time data acquisition rate should be higher than 100 Hz for inertial sensors and 50 Hz for pressure sensors [13]. This is because failure at this point is quite serious. The wireless communication network must maintain connectivity throughout the launch process despite interference from factors such as electromagnetic waves and changing network topography [14]. These sensor nodes must operate without battery changes during the launch period [15]. The system is built to withstand shocks and vibrations during launch by having appropriate packaging and mounting mechanisms. Environmental protection includes IP67-standard protection against moisture, temperature extremes, and EMI [16]. The monitoring display is designed to show different data feeds at once for quick detection of any launch problems.

2.2 Hardware components

The hardware architecture consists of several key elements chosen for their efficiency, effectiveness, and suitability for severe environmental conditions. The system uses a highly precise MEMS-based IMU consisting of 3 accelerometers, gyroscopes, and a magnetometer to provide complete orientation through sensor fusion techniques. The hardware has an acceleration range of ±16 G and ±2000°/sec for the gyro, with 16-bit analog-to-digital resolution. The piezoresistive pressure sensors monitor the pressure profiles in each individual airbag during launch operation [17]. The range of 0-1.5MPa for pressure measurements is adequate considering the pressure profiles of the airbag and surges in pressure. Temperature drift is handled through built-in temperature compensation circuits, and the output is a 4-20 mA current loop. The STM32F4 series ARM Cortex-M4 microcontroller powers each sensor node to collect data locally, process it, and manage the wireless communication. It runs at 168 MHz, and its floating-point unit can perform real-time sensor fusion algorithm calculations. It supports multiple high-speed serial interfaces for communication with sensors and wireless modules.

The CC2530 solution provides an economical solution to connect to the Zigbee network. The 2.4 GHz frequency range has decent propagation characteristics in the industrial environment. The adjustable output power, up to +4.5 dBm, supports effective communication, while the receiver sensitivity for effective reception is -97 dBm. The battery is rechargeable, with energy storage ranging from 2000 to 5000 mAh. In addition, Table 1 shows that the hardware components support more than 12 hours of constant surveillance mode.

Table 1. Main hardware component specifications

Component	Model/Type	Key Specifications
IMU Sensor	MEMS 9-axis	±16g accel., ±2000°/s gyro, 16-bit ADC
IMU Sensor	MPU-9250 MEMS 9-axis	±16g accel., ±2000°/s gyro, 16-bit ADC; Factory calibrated, on-site temperature compensation
Pressure Sensor	Honeywell HSC series piezoresistive	0-1.5 MPa range, 4-20 mA output; Calibrated every 6 months, pre-launch zero adjustment
Pressure Sensor	Piezoresistive	0-1.5 MPa range, 4-20 mA output
Microcontroller	STM32F4 (ARM Cortex-M4)	168 MHz, FPU, 12-bit ADC
Wireless Module	CC2530 Zigbee	2.4 GHz, +4.5 dBm Tx, -97 dBm Rx
Battery	Li-Po	2000-5000 mAh, 12+ hours operation

2.3 Sensor network topology

Network topology design is critical for sensor coverage, communication reliability, and system complexity [18]. The hierarchical architecture uses logical clusters, each containing 5-8 sensor nodes managed by a cluster-head node responsible for data aggregation and routing [19]. Cluster-heads collect data from member nodes via low-power links and forward aggregated data to the gateway using high-power transmission. The recommended number of sensor nodes in a cluster is 5–8 (Figure 2). Sensor placement ensures complete attitude coverage. At least three IMU-equipped nodes are positioned along the longitudinal centerline (forward, amidships, aft) to measure pitch angle [20]. Additional lateral nodes (port and starboard) measure roll angle. Pressure sensors are co-located with IMU nodes. Mesh networking provides redundancy, allowing automatic route reconfiguration around failed nodes [21]. Cluster-head nodes are selected dynamically based on a weighted scoring function combining residual battery capacity (40% weight) and received signal strength indicator (RSSI, 60% weight) to the gateway. Nodes having less than 30% battery level are not considered eligible to become cluster heads. Re-election occurs either every 10 minutes or if the RSSI of the existing cluster head falls below -85 dBm. Gateway handover is initiated if three beacon responses time out (each having a 500 ms timeout). During gateway handover, sensor nodes buffer 50 packets of sensor data to maintain data continuity.

For the 1500-2000 DWT cargo ship experiments, a total of 23 nodes were placed as follows: 6 nodes equipped with IMUs along the longitudinal line (3 ahead, 2 midship, 1 astern) with intervals of 8-12 m for measurement of the pitch angle; 4 IMU nodes located laterally (2 on the port side, 2 on the starboard side) around the maximum width of the vessel for estimation of the roll angle; 13 nodes fitted with pressure sensors located on contact surfaces between the hull and airbags, more densely (2-3 m intervals) near predicted high stress regions around the bow and stern regions, and 4-5 m intervals in midship regions.

3. Communication and Data Acquisition System

3.1 Wireless communication protocol

The wireless communication protocol choice considers range, data rate, energy consumption, and maturity. Zigbee is chosen due to its IEEE 802.15.4 technology, low energy consumption, protocol stack efficiency, and mesh network support [22]. The 250 kbps data rate meets the sensor network bandwidth requirement of up to 50 kbps. LoRa has good range and low data rates not appropriate for high-frequency sampling. Wi-Fi has high throughput but requires much higher power consumption than Zigbee [23]. Working in the 2.4 GHz spectrum shared by Zigbee and Wi-Fi causes negligible interference in the shipyard environment compared to dense urban zones. Zigbee's mesh networking ensures path diversity, which is necessary to keep the network connected as the ship moves through the slipway. The Zigbee application profile enables customized message exchanges in the sensor network [24]. TDMA scheduling within each cluster prevents transmission collisions and enhances protocol performance [25].

Nodes transmit during designated time slots and sleep during idle periods to conserve battery power. The TDMA frame is set to 100 ms to support 100 Hz sampling for inertial sensors, plus beacon and acknowledgment messages. The bandwidth requirements were calculated to verify that Zigbee's 250 kbps data rate is sufficient for the multi-node real-time monitoring system. Each sensor node transmits data once per 100 ms TDMA frame. For IMU sensors sampled at 100 Hz, one sample per frame includes 3-axis accelerometer, 3-axis gyroscope, and 3-axis magnetometer readings (9 values × 2 bytes = 18 bytes). Pressure sensors sampled at 50 Hz contribute 1 sample every 2 frames, averaging 2 bytes per frame. Including the node ID, timestamp, and Zigbee application-layer headers, the total payload is approximately 30 bytes per node per frame. For 23 nodes, the aggregate data rate is 23 nodes × 30 bytes / 0.1 s = 6,900 bytes/s ≈ 55.2 kbps. Accounting for Zigbee protocol overhead (MAC-layer acknowledgments, beacon frames, inter-frame spacing), which adds about 30–40% overhead, the effective required bandwidth is about 75 kbps, well below the 250 kbps raw data rate. The coordinator maintains time synchronization through periodic beacon frames transmitted at the start of each TDMA cycle. Each node's transmission slot is 4 ms long, with 0.5 ms guard intervals to prevent collisions due to clock drift. This allocation provides sufficient margin for the average Zigbee packet transmission time of approximately 2–3 ms for 30-byte payloads at 250 kbps, ensuring reliable slot-based communication without overlap.

3.2 Data acquisition architecture

The data acquisition architecture covers all stages of the process, from sensor data acquisition to reception at the monitoring center via wireless communication. Figure 3 shown below illustrates the pipelining performed by each sensor node, which involves data acquisition, data preprocessing, and communication. The data acquisition process begins when the microcontroller initiates simultaneous sampling of all sensors. Data acquisition from IMUs is performed using SPI/I2C communication interfaces operating at clock speeds not exceeding 10 MHz, whereas data acquisition from the pressure sensor is done using analog channels with DMA support.

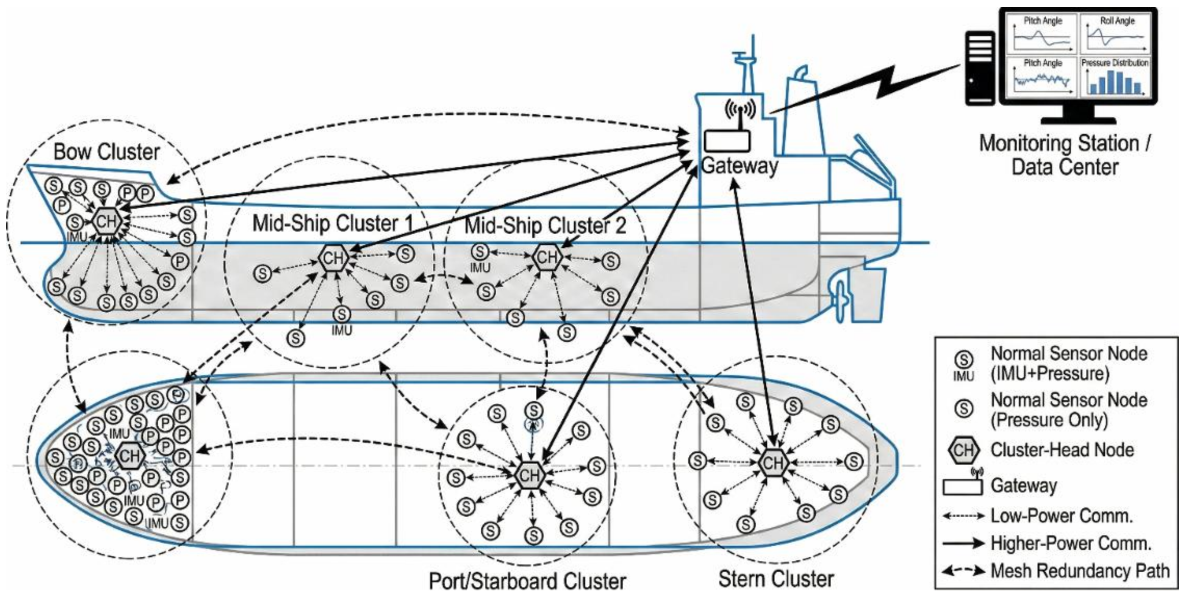

Figure 2. WSN-based monitoring system architecture

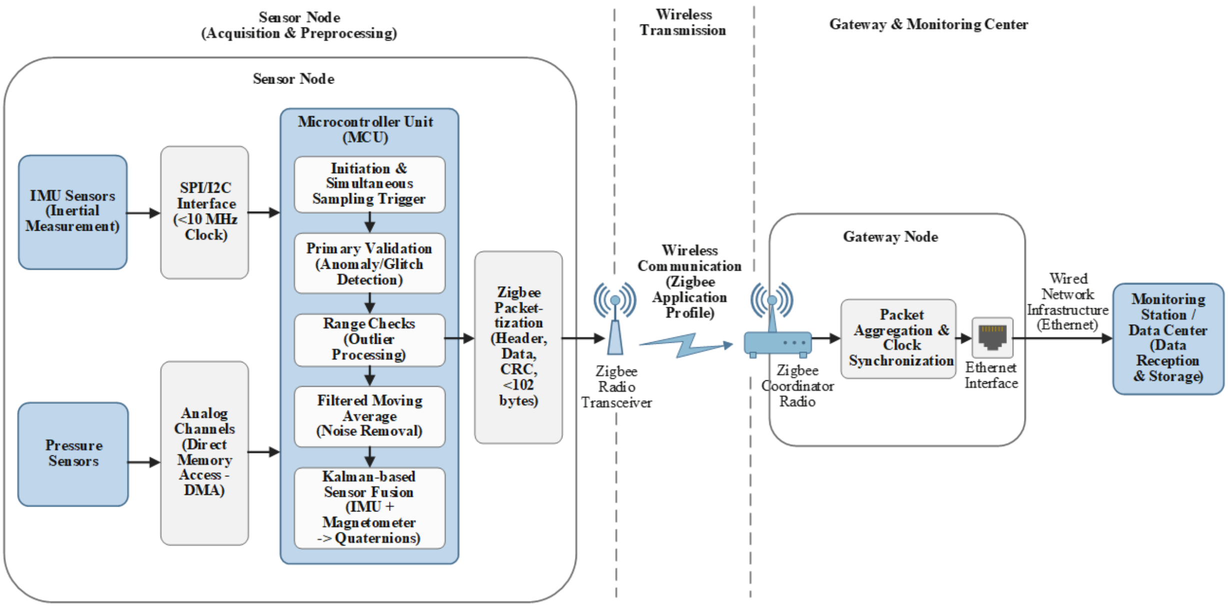

Figure 3. Data acquisition architecture and processing pipeline

The data obtained from the sensors is first validated by considering anomalies that may result from electromagnetic interference, sensor failure, or communication problems [26]. Range tests are performed to check whether the sensor data is realistic, with outliers treated individually. The filtered moving average helps remove noise from the measurement data, but not the dynamic variation in the data. Inertial sensors use Kalman-based algorithms to fuse data with magnetometer data to calculate orientation using quaternions. The formatted data is then wrapped so it can be organized into packets according to the structure provided by the Zigbee application profile. This packet consists of header information containing the source node ID, sequence no., and timestamp, followed by the sensor reading and calculated values, in packets that do not exceed 102 bytes. Gateway nodes connect the WSN to the wired networking infrastructure using Ethernet. Gateway nodes have a dual-interface design with a Zigbee coordinator radio and an Ethernet interface [27]. Data packets received from gateway nodes are assembled into packets that will be sent to the monitoring center with the help of a clock synchronization service.

3.3 Data Processing Pipeline

All information collected by the sensor units is transmitted to the main control center through gateway systems, where various analytical methods are employed to extract important data about the vessel's dynamic behavior during launching. During the initial stages of processing, data fusion across sensor nodes is used to obtain a comprehensive description of the ship's dynamics, rather than individual data points. The ship's pitch angle is obtained using linear regression analysis of the vertical location and angles from IMU sensor nodes positioned in line along the ship to account for the mounting geometry. Similarly, the ship's roll angles are derived from sensor data points depicting lateral angles. Kalman filtering algorithms are applied to the fused attitude information to minimize measurement noise and provide the best state estimates based on sensor data and the ship's dynamic model.

Based on the basic ideas of Newtonian mechanics, a state-transition matrix is constructed from the dynamic correlations among elements of the state vector, such as pitch and roll angles, heave points, and their time derivatives and accelerations [28]. A sensing matrix expresses the information obtained by the sensors in terms of state variables and can also be used to transform coordinates from sensor coordinates to the body-fixed reference frame. The Kalman filter is generally a very good estimator of the state of a system with both measurement and model errors. The Kalman filter is more effective than the simple moving average technique because it dynamically combines multi-sensor information while accounting for process dynamics and noise characteristics. The Kalman filter [28] recursively estimates the ship's attitude and motion state through a two-step process. The prediction step computes the priori state estimate and error covariance:

$$\hat{x}_{k|k-1} = F_k \hat{x}_{k-1|k-1} + B_k u_k \tag{1}$$

$$P_{k|k-1} = F_k P_{k-1|k-1} F_k^T + Q_k \tag{2}$$

Where F_k represents the state transition matrix, B_k is the control input matrix, u_k denotes control inputs, and Q_k is the process noise covariance. The measurement update step incorporates sensor observations to refine the estimate:

$$K_k = P_{k|k-1} H_k^T (H_k P_{k|k-1} H_k^T + R_k)^{-1} \tag{3}$$

$$\hat{x}_{k|k} = \hat{x}_{k|k-1} + K_k (z_k - H_k \hat{x}_{k|k-1}) \tag{4}$$

$$P_{k|k} = (I - K_k H_k) P_{k|k-1} \tag{5}$$

Where K_k is the Kalman gain, H_k is the measurement matrix, R_k represents the measurement noise covariance, and I denotes the identity matrix.

The state vector x_k is defined as:

$$\mathbf{x}_k = [\theta, \phi, h, \dot{\theta}, \dot{\phi}, \dot{h}, \ddot{h}]^T \tag{6}$$

where θ is the pitch angle, ϕ is the roll angle, h is the heave displacement, and the dot notation represents time derivatives (angular velocities and vertical acceleration).
The observation matrix H_k maps the state vector to sensor measurements:

$$\mathbf{H}_k = \begin{bmatrix} 1 & 0 & 0 & 0 & 0 & 0 & 0 \\ 0 & 1 & 0 & 0 & 0 & 0 & 0 \\ 0 & 0 & 0 & 1 & 0 & 0 & 0 \\ 0 & 0 & 0 & 0 & 1 & 0 & 0 \\ 0 & 0 & 0 & 0 & 0 & 0 & 1 \end{bmatrix} \tag{7}$$

corresponding to the direct measurement of pitch, roll, angular rates (gyroscopes), and vertical accelerations (accelerometers).
The process noise covariance Q_k and measurement noise covariance R_k were tuned empirically through iterative field calibration. The diagonal elements of Q_k were set to $\mathrm{diag}(0.01^2, 0.01^2, 0.05^2, 0.1^2, 0.1^2, 0.2^2, 0.5^2)$ in units of degrees^2 and m^2/s^4, reflecting the expected process uncertainty for each state component. The measurement noise covariance $\mathbf{R}_k = \mathrm{diag}(0.3^2, 0.4^2, 0.05^2, 0.05^2, 0.1^2)$ was determined from the manufacturers' specified sensor accuracies (±0.3° for pitch, ±0.4° for roll, ±0.05°/s for gyroscopes, ±0.1 m/s^2 for accelerometers).

To mitigate the drift inherent in double integration of vertical acceleration for heave displacement estimation, we adopted a complementary sensor-fusion approach. Barometric pressure sensors (resolution 0.1 m) were integrated into selected IMU nodes to provide absolute vertical position references. The Kalman filter fuses the barometric altitude with accelerometer-derived heave estimates, using the pressure-based measurement as a drift-correcting constraint in the observation vector z_k (Equation 4). Additionally, pre-launch static calibration establishes the initial accelerometer bias, which is subtracted from all subsequent readings. This sensor fusion approach limits cumulative drift to below 0.5 m over the typical 3–5 minute launching duration, as validated in Section 5.2. The velocity and acceleration graphs can be calculated using the first and second derivatives, respectively, based on filtered data on the vessel's position and orientation, considering the sampling period and the accuracy level used in finite-difference analysis. The instantaneous values of the velocity can be derived from the first derivative, and this is the speed at which the ship is moving on the slipway, along with how the pitch and roll are changing. From the second derivative, we get the acceleration graphs.

The processing algorithm for advanced detection tracks attitude angle, velocity, and acceleration in real time by comparing them against predetermined safety thresholds based on historical ship-launch data. Threshold-based detection rules are: a pitch angle greater than ±8° – indicates Level-1 warning (potential airbag asymmetry); a roll angle greater than ±6° – lateral imbalance (Level-1); a pitch/roll angle rate of change greater than 3°/s – a sudden structural change (Level-2 alert); a vertical acceleration greater than 1.5g or less than 0.2g (without gravity) – abnormal slipway contact dynamics (Level-2); and a pressure differential greater than 0.3 MPa between airbags sensors located next to each other within the same cluster – indicates potential local airbag failure (Level-3 alert). These threshold values are set based on analysis of historical launch data from 2020-2023 from cooperating shipyards (N=47 launches) [29] and reflect ±3 σ boundaries around the parameter distribution. Anomaly detection is a rule-based approach that includes threshold comparison and rate-of-change monitoring methods. This system does not use machine learning classifiers. A statistical process control approach is used as an auxiliary method to visualize gradual degradations in parameters such as airbag pressure loss or friction coefficient increase.

4. Implementation and testing

4.1 System integration

System integration includes hardware assembly, software development, and laboratory testing before system deployment. The sensor-node hardware is built according to the modular design, enabling effective testing, inspection, and repair in the operating environment. Interfaces for the microcontroller, communication, power, and sensors are designed on a custom-made printed circuit board with respect to parameters such as integrity, compatibility, and miniaturization. The design uses four-layer technology; dedicated power and ground layers avoid noise coupling. Component placement accounts for the board's thermal characteristics; power-consuming regulators are located at the edge. The enclosures housing the sensor nodes are made of high-impact ABS, with seals on the lid to protect the system from dust and water entry, targeting IP67-level protection (dust-tight; protected against temporary immersion up to 1 m for 30 minutes per IEC 60529). They feature silicone O-ring seals and cable glands, which help them meet IP67 design requirements. However, official third-party IP67 testing (based on standards set out in IEC 60529, including immersion and dust test procedures) has not yet been performed. Nonetheless, practical proof of waterproofing during field installation, which took place in five launches (with exposure to rain in two cases and splashing during ship cleaning), with no moisture found inside after launch, does not provide any official IP67 certification. The base mounting systems are designed to fix the box safely to the ship surface through welding or bonding because the ship surface is uneven [30]. The cable glands ensure a secure, dust-tight feed-through for the external sensor connector pins.

Software development follows an iterative process that starts with device drivers for sensor interfacing, progresses to communication protocols, and ends with application-layer software. The low-level sensor firmware, written in C using the ARM GCC toolchain, is supported by hardware abstraction layer libraries from the microcontroller manufacturer, which help accelerate development while remaining portable. Support from real-time operating systems like FreeRTOS is very helpful for task, interrupt, and resource management with defined timing constraints. For the system used in ground station surveillance, the program uses Python with libraries such as NumPy for numerical operations, SciPy for signal processing, and PyQt for GUI design [31]. The software uses a modular architecture to separate concerns across modules such as ground station communications, data logging, real-time data processing, GUIs, and alarms. It uses GUIs with timeline data for angles, pressure, velocity, and accelerations, with features like zooming and panning for detailed analysis. The historical data interface includes former launch operation functionalities for data review.

4.2 Field Testing Setup

Field validation testing will be done in actual situations where ships are launched in cooperating shipyards so realistic data can be collected and tested. The validation campaign was conducted over a six-month period (May–October 2024) across five independent ship launching events at cooperating shipyards in Huludao and Tongling, China. The test matrix consisted of three 1500 DWT cargo vessels and two 2000 DWT cargo vessels, each equipped with twelve airbags for launching. The environmental parameters included ambient temperatures between 18°C and 32°C, relative humidity between 55% and 85%, and electromagnetic interference from RF background power at 2.4 GHz, measured between -92 dBm and -78 dBm. All five launches were completed successfully with full data acquisition; no sensor node failures or network outages occurred during the launch processes, though one pre-launch hardware check identified a faulty pressure sensor connector that was replaced before the trial commenced. The first involves launching a 1500 DWT cargo ship using twelve airbags on its bottom. The nodes will be strategically positioned based on the topology design, while ensuring safe placement that protects them from damage during the launching process. This includes nodes with an inertia measurement unit and others placed at the front position, three between and mid-way positions, as well as additional pressure-measuring nodes.

The sensors are activated several hours before launch operations begin to check communication connectivity and confirm the system works correctly in an inactive state. Standard values are recorded when the vessel remains stationary at the launch cradle, serving as a baseline for future comparison of motion data to determine sensor drift errors. The monitoring site is established in a temporary tent near the slipway, with communication to the launch area through gateway devices, processing computers, and operator interfaces. Redundant power and communications systems ensure continuous operation if electric power fails during the launch process. At the start of the launch procedure, it is important to measure the pressure of the inflated airbags using the sensors to verify proper loading and identify any airbags that do not reach the required pressure. As pressure increases, weight transfers from the cradle to the airbags [32]. Once the airbags reach the required pressure, the blocks restraining their movement are released, allowing the ship to move down the ramp under gravity. At the same time, the monitoring system measures attitude changes, velocity, and acceleration at frequencies of 100 Hz and 50 Hz, respectively.

5. Results and analysis

From the performance figures in Table 2, the system shows consistent performance across all five test runs. The end-to-end latency averaged 35.2 ms, with a low standard deviation of 8.1 ms, showing that real-time communication is possible. Packet delivery rate exceeded 99% in all test runs, proving that the Zigbee mesh network is reliable even in the shipyard electromagnetic environment. Heave displacement drift was contained to 0.38±0.15 m over the 3.1–5.4 minute launch durations, demonstrating the effectiveness of the sensor fusion approach described in Section 3.3. The following subsections provide detailed analysis of representative data from individual launches.

5.1 Attitude data acquisition

This series of field tests provides the data sets needed to analyze all attitudes that occur during the launch process of various ships at different times. The attitude angle data demonstrates a normal distribution that corresponds to the physical processes occurring during each ship launch. At first, during inflation, the ship's weight starts to transfer from its cradle to the air bags. During this time, all attitude angles undergo minor fluctuations but remain essentially constant due to pressure imbalances and the settling of the ship's hull onto the air bags. There occurs a minor bow-up attitude of the pitch angle equal to 1° - 2° due to the position of its center of gravity. As the launching sequence continues and the vessel begins to move along the slipway, large attitude variations occur due to dynamic equilibrium of forces and momentum exchange. The pitch attitude varies widely, from +5 to -3 degrees, as the vessel accelerates or decelerates due to changes in friction force, air bag deflation, and the components of gravitational force due to the slipway's inclination. Pitch attitude variations can be as high as 3 to 4 degrees per second during dynamic attitude changes, requiring high-resolution sensors for accurate measurements. Variations in the roll attitude are smaller than ±1.5 degrees for normal launch of vessels along the slipway.

Table 2. Summary statistics across five field trials

Performance Metric	Mean	Std. Dev.	95% CI	Min–Max
End-to-end latency (ms)	35.2	8.1	[31.4, 39.0]	22–58
Packet delivery ratio (%)	99.6	0.3	[99.4, 99.8]	99.1–99.9
Pitch angle accuracy (°)	±0.28	0.09	[±0.24, ±0.32]	±0.18–±0.41
Roll angle accuracy (°)	±0.35	0.11	[±0.30, ±0.40]	±0.22–±0.48
Pressure measurement error (% FS)	1.3	0.4	[1.1, 1.5]	0.8–2.1
Heave displacement drift (m)	0.38	0.15	[0.29, 0.47]	0.21–0.62
System operational duration (min)	4.2	0.8	[3.7, 4.7]	3.1–5.4

The attitude angle time histories of a typical launching operation of a 2000 DWT ship are shown in Figure 4 in order to illustrate the overall trend of pitch, roll, and heave motions during the launching operations. There is a good level of consistency of measurements from various sensors. This means the system is performing well in terms of the measurements made, and the sensor fusion process is effective. The difference between measurements in various positions along the length of the vessel is just a matter of actual deformation of the vessel in the process of launching it. The displacement measurements in relation to Heave refer to the downward movement of the displaced vessel as it moves down the slipway and enters into water. At the same time, displacement values of 3 to 5 meters are measured based on slipway dimensions and the launching setting design. The heave velocity increases continuously, reaching a peak of 2 to 3 m/s as the vessel reaches its maximum speed in the middle part of the slipway (Figure 5). Negative heave acceleration, not higher than 4 m/s^2, is measured as it slows to a stop upon entering the water.

5.2 System performance evaluation

The system's performance characteristics are analyzed by assessing data quality, communication reliability, and performance across operating scenarios. Sampling frequencies are met or exceeded; both the IMU data stream and pressure data stream update at 100 Hz and 50 Hz, respectively, during all phases of launch. Moreover, latency from data collection to system readiness at the monitoring station averages 35 milliseconds, with the 95th percentile not exceeding 60 milliseconds. Measurement accuracy is determined using independent reference measurements and consistency analysis of measurements performed by redundant sensors. Comparisons between the attitude angle measurements of the WSN system and those of a VectorNav VN-100 inertial navigation system (factory-specified accuracy ±0.1° for pitch/roll), which served as the ground-truth reference, show that the RMS differences for the pitch and roll measurements during dynamic tests are 0.3° and 0.4°, respectively. The VN-100 was mounted at the ship's centerline amidships alongside WSN node #8 and recorded data synchronously during all five launches, providing over 10,000 measurement pairs per trial for statistical validation. This demonstrates that these readings are well within ±0.5° accuracy specifications and shows that, although extremely inexpensive, MEMS-based sensors provide performance features nearly as good as tactical-grade inertial sensors at a very low cost. Pressure measurement accuracy is verified using precision reference measurements with Fluke 718-300G portable pressure calibrators (±0.05% reading accuracy), and differences of ±1.5% full scale or ±22.5 kPa are found for the 1.5 MPa range sensors used. Statistics on communication reliability show good wireless connectivity throughout the launch process, despite the hostile electromagnetic surroundings and constantly changing network topology. Information transfer of more than 99.5% is guaranteed across all sensors during normal operation; the ad-hoc network feature ensures it can bypass all possible link failures. Gateway transfers during vessel translation along the slipway occur with a delay of no more than 200 milliseconds, and data buffering does not cause data loss. Power analysis shows all devices meet expected lifetimes; the sensors operate for more than 15 hours on a single battery charge.

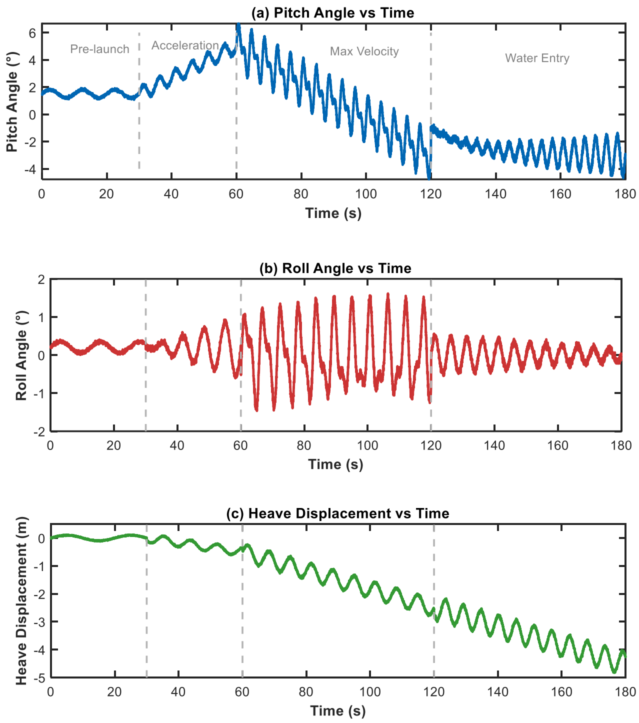

Figure 4. Attitude angle time series during ship airbag launching

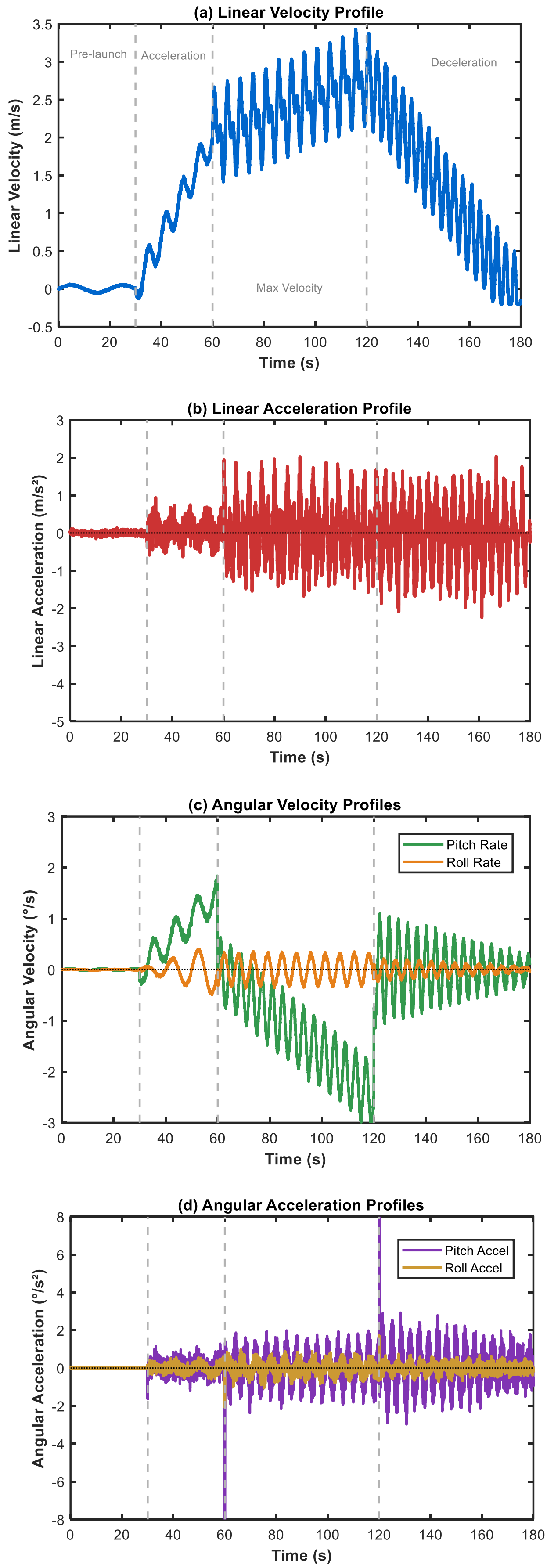

Figure 5. Velocity and Acceleration Profiles During Ship Airbag Launching

The shipyard electromagnetic environment included active welding operations (arc welders at 200–400 A), overhead cranes with variable-frequency drives, and extensive metal structures. Background RF interference at 2.4 GHz ranged from -92 dBm (open areas) to -78 dBm (near welding, <10 m). RSSI between nodes and gateway varied with distance: >-70 dBm at <30 m (PDR >99.8%), -70 to -82 dBm at 30–60 m (PDR >99.3%), and -82 to -88 dBm at 60–90 m (PDR >98.5%). Mesh routing maintained connectivity during line-of-sight obstructions with <2 s reconfiguration time. Peak interference events (welding arc strikes within 5 m) caused temporary 8–12 dB RSSI drops (100–300 ms duration), mitigated by TDMA timing and MAC-layer retransmission, with zero packet loss recorded during such transients. Table 3 presents performance measures of the developed monitoring system to meet the specifications and show improvement over existing monitoring systems. The WSN system's high resolution and fast response time helped resolve transitory events better than would have been possible with conventional systems.

Table 3. System performance metrics

Performance Metric	Specification	Achieved Value
IMU Sampling Rate	≥100 Hz	100 Hz
Pressure Sampling Rate	≥50 Hz	50 Hz
End-to-end Latency	<100 ms	35 ms (avg), 58 ms (95th percentile)
Pitch Angle Accuracy	±0.5°	±0.3° (RMS)
Roll Angle Accuracy	±0.5°	±0.4° (RMS)
Pressure Accuracy	±2% FS	±1.5% FS (±22.5 kPa)
Packet Delivery Rate	>98%	99.5%
Node Battery Life	>12 hours	15+ hours
Number of Sensor Nodes	20-25	23 (typical deployment)
Communication Range	>100 m	120 m (line-of-sight)
System Response Time	<5 s	<2 s (from anomaly to alert)

The current monitoring system focuses primarily on real-time data acquisition, visualization, and threshold-based anomaly detection. However, the rich historical datasets accumulated from multiple launch operations present opportunities to develop predictive analytics capabilities. Drawing parallels with recent advances in autonomous intelligent prediction models—where deep learning techniques are trained on historical patterns to forecast future behaviors- future iterations of this system could employ similar approaches to predict launch trajectories, anticipate potential anomalies, and optimize operational parameters.

5.3 Comparative analysis

It is possible to compare the suggested WSN system with existing systems using mechanical pressure gauges, and the results show certain superiority from various points of view. The localization ability of the sensor network is definitely superior compared to that of ordinary systems: whereas a 3-5-meter distance between gauge sensors allows the measurement of local pressure changes and attitudes that are totally invisible for regular systems with 15-20 meters distance, 3D attitudes are a completely new stage that goes far beyond the limitations caused by any number of sensors used in regular pressure gauges. Another area where significant improvements have been observed is temporal resolution, or response time, where the 100 Hz sampling frequency of the 100 Hz IMU helps determine events that occur within time scales of tens of milliseconds in case of transient processes whereas in case of mechanical sensors whose responses are dominated by their own inertia and damping, the response time is measured in hundreds of milliseconds to a few seconds. This is beneficial for detecting impulse events like friction bursts, airbag bursts, or impacts on structures, allowing early detection of potential problems that require immediate action.

A significant benefit of this wireless design is that it requires much less installation time and costs less because it eliminates wires connecting sensors and actuators over long distances in the difficult conditions of a shipyard. Also, the sensors are easily movable and therefore adaptable to any type and size of ship, because there is no fixed mounting point for the gauges, which improves adaptability and flexibility. The lack of wires also eliminates a primary cause of downtime by removing the need to diagnose potential wire malfunctions. Table 4 compares the performance parameters of the traditional monitoring method with those of the designed WSN system. It is revolutionary to monitor pressure distribution, three-dimensional attitude angles, velocity, and acceleration simultaneously, as this provides opportunities not only to improve safety but also to optimize the ship-launching process. However, the more complex functionalities provided by the WSN monitoring system are not only about progressive system development but also about creating a paradigm shift in launch strategy and process planning. The extensive collection of attitude and pressure data can be integrated into a mathematical model to evaluate and improve conceptual designs and launch performance predictions. The databases created from multiple launches can be used for statistical analysis of performance parameters and to identify exceptional points related to system malfunctions.

To ensure transparency of the reported improvements, the calculation basis for each performance metric is detailed below. The 75% reduction in spatial blind spots is derived from comparative spatial coverage analysis assuming a 40 m hull-airbag contact length representative of the 1500-2000 DWT vessels tested. Traditional systems employ 3 mechanical pressure gauges at 20 m spacing, leaving two 15 m blind zones (30 m total, or 60% of the contact surface). The WSN system deploys 13 pressure-sensing nodes with 3–5 m spacing in high-stress zones (bow, stern) and 4–5 m spacing at midship sections, reducing blind zones to approximately 6 m (15% of contact surface). The reduction is calculated as (60%−15%)/60% = 75%. The 20–100× improvement in temporal resolution compares the WSN system's digital sampling rates (50 Hz for pressure, 100 Hz for IMU) against mechanical gauge/analog chart recorder rates of 1–5 Hz, documented in shipyard archived launch records from 2020–2023 at the cooperating facilities. The ratio range spans 50/5 = 10× (best case for mechanical) to 100/1 = 100× (worst case for mechanical), with typical improvement approximately 20–50×. This 85% reduction in installation time is based on deployment tests conducted in three separate tests for each system type. The conventional wired system took 19.5±2.5 hours on average (18 to 22 hours), mainly consisting of cable runs within conduits (~70% of the total setup time), followed by gauge installation, connection, calibration, and connectivity tests.

Table 4. Comparison of traditional and WSN-based monitoring systems

Characteristic	Traditional Mechanical Gauges	WSN-Based System	Improvement	Basis
Spatial Coverage	15-20 m gauge spacing (60% blind zones)	3–5 m node spacing (15% blind zones)	75% reduction in blind spots	3 gauges at 20 m spacing vs. 23 nodes at 3–12 m spacing; 40 m contact length
Measurement Types	Pressure only	Pressure, attitude, velocity, acceleration	Comprehensive multi-parameter monitoring	System design specifications
Temporal Resolution	1-5 Hz (limited by mechanical response)	50-100 Hz (digital sampling)	20-100× faster response	Shipyard archived launch records (2020–2023)
Installation Time	19.5±2.5 h (cable installation)	3.0±0.5 h (wireless deployment)	85% reduction	Timed deployment tests (N=3 per system)
Real-time Visualization	Manual gauge reading and recording	Automated graphical dashboard	Instantaneous operator awareness	Operational procedure comparison
Data Logging	Manual recording or discrete loggers	Continuous synchronized recording	Complete historical record	Data acquisition protocol
Measurement Accuracy	±3-5% FS (gauge quality dependent)	±1.5% FS (calibrated digital)	50% improvement	Reference calibrator validation
System Flexibility	Fixed installation	Reconfigurable modular nodes	Adaptable to different vessels	Deployment observation across 5 trials
Maintenance Requirements	Periodic gauge calibration	Battery replacement only	Reduced maintenance burden	6-month field operation log
Post-operation Analysis	Limited data availability	Comprehensive time-series data	Detailed trajectory reconstruction	Data storage architecture

The WSN system took only 3.0±0.5 hours (2.5 to 3.5 hours), including magnetic/welded bracket installation, power-on testing, and formation of a Zigbee Mesh network. The reduction is calculated as (19.5–3.0)/19.5 = 84.6% ≈ 85%. Although the above comparisons show significant benefits over conventional mechanical gauges, recent studies have indicated more sophisticated monitoring techniques with intermediate performance. The applications of fiber-optic sensors in SHM were investigated by Li et al., who have pointed out the fact that the common spatial resolution of FBG sensors is 10- 15 m with a sampling frequency of 10- 20 Hz. However, such monitoring requires 6-8 hours of fiber routing without attitude measurements [33]. Lynch and Loh summarized wireless sensor network implementations for structural monitoring, reporting typical node spacing of 8–12 m and sampling rates of 5–10 Hz, demonstrating wireless feasibility but without integration of inertial sensors for comprehensive attitude tracking [34]. Compared to these recent systems, the proposed WSN architecture achieves 50–62% further improvement in spatial coverage (3–5 m vs. 8–15 m spacing), 5–10× higher temporal resolution (50–100 Hz vs. 5–20 Hz), and uniquely integrates multi-axis IMU measurements for comprehensive 3D attitude monitoring—capabilities not reported in prior wireless or fiber-optic ship launching systems. Installation time (3.0 h) represents a 25–50% reduction compared to FBG systems (6–8 h) while maintaining cost competitiveness (estimated 2–3× traditional system cost vs. 8–12× for FBG solutions).

6. Conclusion

This research paper introduces an innovative monitoring system to control airbag launching processes for large ships using WSN technology to address major limitations of traditional gauge systems. This system efficiently integrates various sensor types, including IMUs and pressure sensors, into the network design to provide reliable monitoring of the airbag launching process at all levels, enabling efficient analysis and visualization at any desired level. The suggested system incorporates a hierarchical Zigbee network topology to address industrial-environment challenges, such as electromagnetic interference, while improving power efficiency by implementing TDMA protocols. Algorithms are applied to improve the accuracy of the overall measurement process. Field testing under real-life launch conditions confirmed that it meets the stated performance characteristics. These include attitude angle measurement with an accuracy of less than ±0.5°, pressure measurement with an error of ±2% of full-scale, and total latency lower than 60 ms with 95% probability. The transient response characteristics captured by the 100 Hz sampling rate of the Inertial Measurement Unit on board the vehicle are not normally available from typical monitoring systems. This comparative analysis demonstrated extremely favorable features compared to traditional mechanical equipment. There were several aspects where the offered system exhibited considerable advantages: 75% decrease in monitoring of blind zones (from 60% to 15% for the hull) through spacing 3-5 meters of nodes in contrast to 15-20 meters of traditional gauges; 20-100× faster data acquisition (from 50-100 Hz in contrast to 1-5 Hz), which made it possible to monitor any temporary events; and 85% saving of time of installation (3.0 hours instead of 19.5 hours) owing to the absence of any cable system. There are a number of limitations with respect to this study. Firstly, the field validation process involved a limited number of launches, amounting to only five launches taking place at two shipyards where the conditions experienced were moderate, specifically, no rainfall and warm weather conditions. Testing for performance under extreme conditions such as strong winds, sub-zero temperatures, and heavy rainfall has not yet been conducted. Second, the study was limited to ship sizes of 1500-2000 DWT; testing for larger vessels (over 5000 DWT), which would involve longer slipway launches, is still to be conducted. Third, testing sensor drift, battery wear, and enclosure sealing performance over many years of deployment was limited because the test duration was only six months. No standard environmental qualification tests were conducted in accordance with IEC and ASTM standards, which involve vibration and thermal shock, salt fog exposure, among others. Future research directions to be explored

using the dataset built up through five launches (12+ hours of synchronized multi-sensor data collection spanning 52 launches combined with the 2020-2023 archive) include:
(1) Predictive trajectory modeling: Construct LSTM (Long Short-Term Memory) neural networks using the 52-launch data set that will be used for predicting changes in the pitch/roll angle, heave displacement, and pressure in the airbags for the first 30 seconds of contact with the slipway. The predictive time-series model would enable early identification of trajectory anomalies (such as lateral deviation >2 m by t=15 s) that lead to inevitable structural impact with the slipway walls, giving operators 10–15 seconds to brake.
(2) Transfer Learning for Scalability of Vessels: Employing transfer learning to tune the threshold and parameter settings of the Kalman filter, which are tuned for 1500 to 2000 DWT vessels, to higher DWT vessels (3000-10,000 DWTs) using few training data (N=3 to 5 launches per new class). This will minimize the effort required to validate the model across different vessel domains and airbag types.
(3) Feedback control for closed-loop pressure management of airbags: Utilize the real-time pressure data from the WSN system to develop a feedback mechanism to adjust the inflation rate of airbags during the launch process. This could be achieved by controlling the pressure difference between the bow and stern clusters to below 0.2 MPa, based on the load distribution obtained via the IMU.
(4) Sensor fusion using strain gauges and acoustic emissions: Extend the existing IMU-pressure sensor network to include fiber Bragg grating strain sensors (10-15 nodes), along with piezoelectric acoustic emission sensors (4-6 nodes), to detect micro-cracking, welding stress, and vibrations due to friction that are beyond the capabilities of inertial/pressure sensor networks alone. Multi-sensor fusion would result in the detection of structural failures (for example, airbag seam tear and hull plate buckling) in 5-10 seconds prior to catastrophes.
(5) Integration of digital twin: Integrate the WSN-based data acquisition system with the finite element analysis (FEM) models of ship-airbag-slipway interactions, which will allow real-time updates to the model (Bayesian parameter estimation) during the process of the ship launching. The calibrated digital twin will provide stress-field information in areas not being measured, helping assess post-launch integrity and optimize the process.
The method could also be applied to launching offshore platforms and constructing vessel docks, as well as to industrial applications requiring the lifting of bridge segments and the transport of large equipment.

Ethical issue

The authors are aware of and comply with best practices in publication ethics, specifically regarding authorship (avoidance of guest authorship), dual submission, manipulation of figures, competing interests, and compliance with research ethics policies. The authors adhere to publication requirements that the submitted work is original and has not been published elsewhere. All survey participants provided informed consent before participating, and the anonymity and confidentiality of all respondents were strictly maintained throughout the research process.

Data availability statement

The manuscript contains all the data. However, additional data will be provided by the corresponding author upon reasonable request.

Conflict of interest

The authors declare no potential conflict of interest.

References

[1] G. Melazzo Filho, P.I.D. Lameira, R. dos Santos Saavedra, T.C.G.M. Filgueiras, L.C. Campos Filho, Comparative study for naval repairs using longitudinal slipway or airbags, Acta Scientiarum. Technology 43 (2021) e51796.
[2] N. Mandlekar, M. Joshi, B.S. Butola, A review on specialty elastomers based potential inflatable structures and applications, Advanced Industrial and Engineering Polymer Research 5(1) (2022) 33-45.
[3] J. Liu, L. Yu, Numerical investigation on nonlinear contact coupling during ship launching process by an array of airbags, Ocean Engineering 255 (2022) 111481.
[4] A. Timothy, M.A. Akintunde, A.R.K. Inkum, Enhancing Safety and Reliability of Marine Airbags for Ship Launching: Failure Analysis and Mitigation Strategies, International Journal of Engineering Research & Technology 12(9) (2023) 1-7.
[5] A.R. Prabowo, T. Tuswan, R. Ridwan, Advanced development of sensors' roles in maritime-based industry and research: From field monitoring to high-risk phenomenon measurement, Applied Sciences 11(9) (2021) 3954.
[6] B.-G. Paik, S.-R. Cho, B.-J. Park, D. Lee, B.-D. Bae, J.-H. Yun, Characteristics of wireless sensor network for full-scale ship application, Journal of marine science and technology 14(1) (2009) 115-126.
[7] C. Han, X. Hu, D. Sun, The influence of ship roll and pitch on absolute measurement of ship heave signals and its correction method, Ocean Engineering 322 (2025) 120468.
[8] M. Abdulkarem, K. Samsudin, F.Z. Rokhani, M.F. A Rasid, Wireless sensor network for structural health monitoring: A contemporary review of technologies, challenges, and future direction, Structural health monitoring 19(3) (2020) 693-735.
[9] A.R. Ahmad, R. Meligy, S. Mekid, Development of a 4-Axis Force Sensor for Center of Gravity Estimation Using Tree-Based Machine Learning Models, IEEE Sensors Journal (2025).
[10] A. Alshuhail, A. Alshahrani, H. Mahgoub, M. Ghaleb, A.A. Darem, N.O. Aljehane, M. Alotaibi, F. Alzahrani, Machine edge-aware IoT framework for real-time health monitoring: Sensor fusion and AI-driven emergency response in decentralized networks, Alexandria Engineering Journal 129 (2025) 1349-1361.
[11] X. Zhou, Y. Yang, Y. Xu, C. Li, H. Ren, A study on the error characteristics and compensation algorithm for strain gauge in ship structure monitoring systems, International Conference on Offshore Mechanics and Arctic Engineering, American Society of Mechanical Engineers, 2022, p. V002T02A022.
[12] H. Murayama, D. Wada, H. Igawa, Structural health monitoring by using fiber-optic distributed strain sensors with high spatial resolution, Photonic Sensors 3(4) (2013) 355-376.

[13] Z. Szczerba, P. Szczerba, K. Szczerba, Sensitivity of piezoresistive pressure sensors to acceleration, Energies 15(2) (2022) 493.
[14] W. Shafik, An overview of computational modeling and simulations in wireless communication systems, Computational Modeling and Simulation of Advanced Wireless Communication Systems (2024) 8-40.
[15] S. Aslam, M.P. Michaelides, H. Herodotou, Internet of challenges, IEEE Internet of Things journal 7(10) (2020) 9714-9727.
[16] K. Ramkumar, B. Singh, L. Pan, A. Sharma, Sensor Technologies and Wireless Communications in Industry 5.0: A Solution for Smart Manufacturing, CRC Press2025.
[17] Z. Si, W. Wei, W. Feng, B. Li. Development and Construction of Intelligent Security Monitoring System, In2020 IEEE 3rd International Conference on Information Systems and Computer Aided Education (ICISCAE) (2020) 335-338.
[18] R.W. Coutinho, A. Boukerche, L.F. Vieira, A.A. Loureiro, Underwater wireless sensor networks: A new challenge for topology control–based systems, ACM Computing Surveys (CSUR) 51(1) (2018) 1-36.
[19] K. Guleria, A.K. Verma, Comprehensive review for energy efficient hierarchical routing protocols on wireless sensor networks, Wireless Networks 25(3) (2019) 1159-1183.
[20] F. Gravenhorst, Rowing Performance Analysis Using Motion Sensors, ETH Zurich, 2015. https://doi.org/10.3929/ethz-a-010406961
[21] A. Adeoye, A Framework for the Self-Configuration of Wireless Mesh Networks, (2009). http://hdl.handle.net/10012/4461
[22] S. Tennina, A. Koubâa, R. Daidone, M. Alves, P. Jurčík, R. Severino, M. Tiloca, J.-H. Hauer, N. Pereira, G. Dini, IEEE 802.15. 4 and ZigBee as enabling technologies for low-power wireless systems with quality-of-service constraints, Springer Science & Business Media2013.
[23] S. Zhao, Y. Yuan, N. Mei, H. Yuan, Design and implementation of a hydraulic balancing system based on low-power ZigBee Ad-Hoc network electric household control valves, Energy 313 (2024) 133867.
[24] H.-C. Lee, K.-H. Ke, Monitoring of large-area IoT sensors using a LoRa wireless mesh network system: Design and evaluation, IEEE Transactions on Instrumentation and Measurement 67(9) (2018) 2177-2187.
[25] E. Shayo, P. Mafole, A. Mwambela, A survey on time division multiple access scheduling algorithms for industrial networks, SN Applied Sciences 2(12) (2020) 2140.
[26] S. Sharma, K. Gupta, D. Gupta, S. Rani, G. Dhiman, An Insight Survey on Sensor Errors and Fault Detection Techniques in Smart Spaces, CMES-Computer Modeling in Engineering & Sciences 138(3) (2024).
[27] H. Qin, H. Chen, N. Li, Y. Deng, G. Yang, Y. Peng, Delay-aware Dual-Interface Gateway Activation for Energy-Efficient Data Collection in IoT, IEEE Transactions on Green Communications and Networking (2024).
[28] R.E. Kalman, A new approach to linear filtering and prediction problems, Journal of Basic Engineering 82(1) (1960) 35-45.
[29] I. Pathirannahalage, V. Jayasooriya, J. Samarabandu, A. Subasinghe, A comprehensive analysis of real-time video anomaly detection methods for human and vehicular movement, Multimedia Tools and Applications 84(10) (2025) 7519-7564.
[30] V.M. Shkolnikov, Hybrid Ship Hulls: Engineering Design Rationales, Butterworth-Heinemann2014. ISBN:9780128103050
[31] C. Patel, N. Garg, S. Panigrahi, V. Kumar, Signal Processing in Real-Life Structural Health Monitoring: MATLAB and Python Implementation, Damage Detection and Structural Health Monitoring of Concrete and Masonry Structures: Novel Techniques and Applications, Springer2025, pp. 273-294.
[32] L. Volenyuk, A. Rashkovskyi, Ship stability analysis during launching from longitudinal sloping slipway by pneumatic airbags, International Shipbuilding Progress 64(1-2) (2017) 41-50.
[33] H.N. Li, D.S. Li, G.B. Song, Recent applications of fiber optic sensors to health monitoring in civil engineering, Engineering Structures 26(11) (2004) 1647-1657.
[34] J.P. Lynch, A summary review of wireless sensors and sensor networks for structural health monitoring, The Shock and Vibration Digest 38(2) (2006) 91-128.